J. Fluid Mech. (1997), *vol.* 343, *pp.* 95–110. Printed in the United Kingdom

© 1997 Cambridge University Press

Formation and stability of liquid and molten beads on a solid surface

By STEFANO SCHIAFFINO† AND AIN A. SONIN

Department of Mechanical Engineering, Massachusetts Institute of Technology, Cambridge, MA 02139

(Received 24 February 1995 and in revised form 13 March 1997)

We present an experimental study of the formation and stability of small-scale beads deposited onto a solid surface by sweeping a droplet stream over it. We are concerned particularly with beads formed from molten droplets deposited on a cold substrate, as in the work of Gao & Sonin (1994), but some results of isothermal deposition are also shown. We show that a molten bead forms with parallel contact lines which have been arrested by freezing while the bead itself is still largely in a liquid state, and that the still-molten material is stable when the contact angle is less than $\frac{1}{2}\pi$ and unstable when it exceeds $\frac{1}{2}\pi$, consistent with Davis's (1980) theory. In addition, we present a relatively simple inviscid theory for small-scale (small Bond number) beads which allows us to compute the wavelength associated with the maximum growth rate of the instability, and show that it agrees with the dominant wavelength in the experiments.

1. Introduction

Theory predicts (Rayleigh 1878; Chandrasekhar 1961), and experiments confirm, that a small-diameter liquid jet in air is always unstable and will break up into a series of distinct droplets. A sessile liquid bead on a flat surface, on the other hand, like the one illustrated in figure 1(*a*), may be unstable or stable, depending on conditions. For example, a bead formed from pure water by drawing the tip of a fine syringe rapidly over a glass surface while ejecting liquid from it will typically be unstable, and will quickly reshape itself into a series of separate, sessile droplets, much like a jet. Other liquid and surface material combinations yield different results: the bead may develop bulges but not separate into pieces, or it may show no signs of instability at all and remain perfectly uniform along its length.

The stability of beads is important in applications where a uniform bead of liquid or molten material needs to be deposited on a solid and allowed to solidify by thermal, chemical, or photochemical means. Instabilities which proceed faster than the solidification mechanism will cause bead non-uniformity. Gao & Sonin (1994), in their investigation of deposition and solidification of molten microdrops, showed that under some conditions uniform beads could be formed by sweeping a droplet generator over the target surface, but that under other conditions the beads would develop exaggerated deformities before they solidified. They described qualitatively the conditions that favoured uniformity of molten beads on subcooled targets, but offered no quantitative theory for the instability.

The conditions for the stability of a small bead have been examined by Davis (1980) and also Sekimoto, Oguma & Kawasaki (1987). The stability of a bead depends on the boundary conditions at its contact lines. Davis used a linearized hydrodynamic theory

† Present address: Hewlett-Packard Española, Barcelona, Spain.

https://doi.org/10.1017/S0022112097005831 Published online by Cambridge University Press

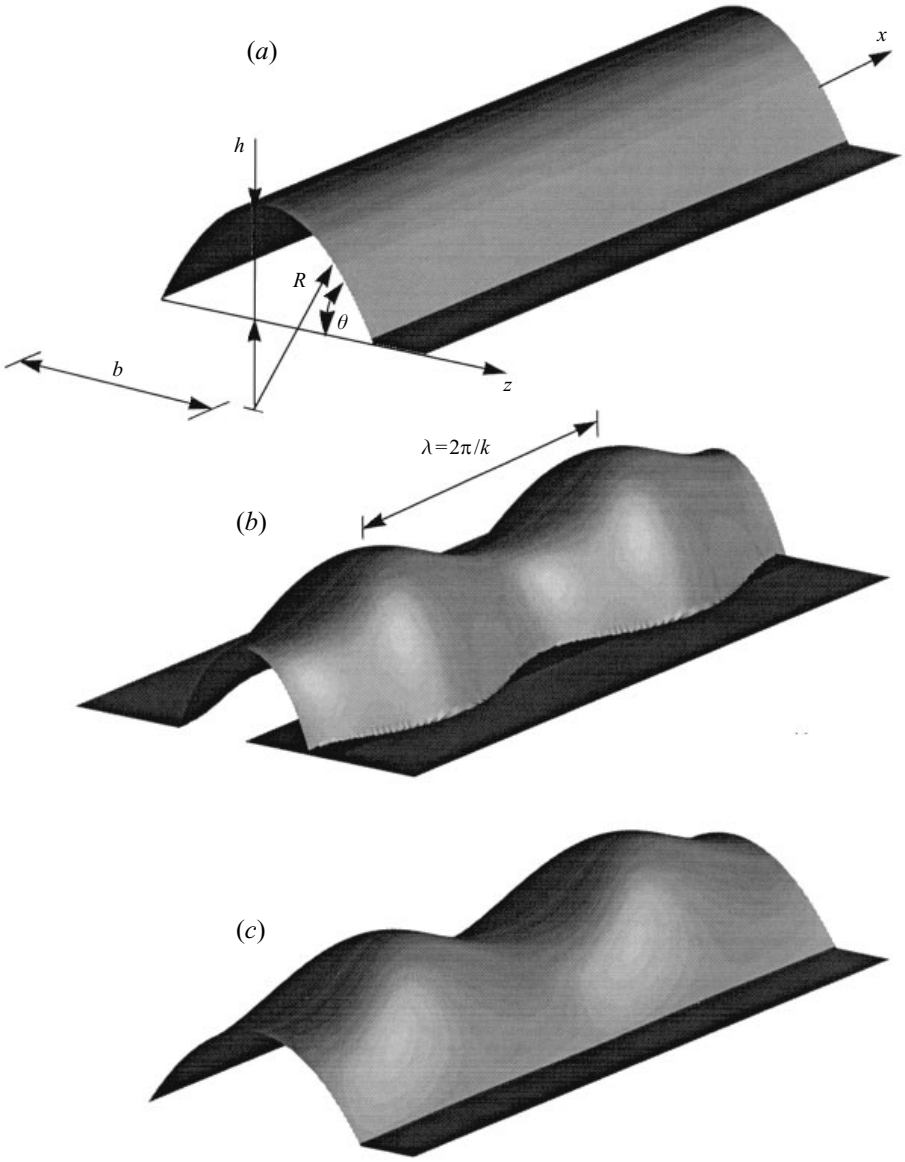


FIGURE 1. Shapes and geometrical parameters for (*a*) an undisturbed bead, (*b*) a perturbed bead maintaining constant contact angle, and (*c*) a perturbed bead with arrested, parallel contact lines.

to derive sufficient conditions for stability for three cases: (*a*) beads whose contact angle θ remains fixed at an equilibrium value while the contact lines are free to move, as in figure 1(*b*); (*b*) beads whose contact angle depends on the contact line speed, but reduces to an equilibrium value at zero speed, and (*c*) beads whose contact lines are arrested in a parallel state while the contact angle is free to change, as in figure 1(*c*). He showed that, like Rayleigh's liquid cylinder, cases (*a*) and (*b*) will always be unstable at some disturbance wavelengths, but that case (*c*) will be stable if $\theta < \frac{1}{2}\pi$. Case (*c*) is representative of a liquid bead with strong contact angle hysteresis.

In this paper, we present an experimental study of the formation and stability of small-scale beads formed by the deposition of a droplet stream onto a surface. We are

https://doi.org/10.1017/S0022112097005831 Published online by Cambridge University Press

concerned particularly with beads formed from molten droplets deposited on a cold substrate, as in the work of Gao & Sonin (1994), but some results of isothermal deposition are also shown for contrast. We show that a molten bead develops parallel contact lines which have been arrested by freezing while the bead itself is still largely in a liquid state, and that the still-molten material develops instabilities when $\theta > \frac{1}{2}\pi$, consistent with Davis's (1980) theory. In addition, we present a relatively simple inviscid theory for small-scale (small Bond number) beads which allows us to compute the wavelength associated with the maximum growth rate of the instability (not provided by Davis's theory), and compare with the dominant wavelength in the experiments.

2. Experiments with molten wax

Gao & Sonin (1994) produced small beads of molten material by sweeping a droplet generator at fixed speed U over a subcooled target while dispensing molten microdrops at a high frequency f (figure 2). The droplets arrived at the target in liquid form. If the dimensionless ratio $f(2a)/\mathrm{U}$, where a is the in-flight microdrop radius, exceeds a value $F(\theta)$ which depends on the contact angle θ of an individual deposited droplet (Gao & Sonin 1994, equation (31)), successive droplets will overlap upon impact and will tend to coalesce and form a continuous bead. Melt solidification commences after contact with the subcooled target, but the solidification front progresses into the melt at a rate much slower than the sweep speed (more on this later) and the bead retains a largely liquid state as it forms. The bead's cross-sectional area can be controlled via the magnitude of the parameter $f(2a)/U$, mass conservation giving $A = (\frac{2}{3}\pi a^2) f(2a)/U$, and the bead's apparent contact angle can be varied via the target temperature, lower target temperatures yielding higher contact angles (Gao & Sonin 1994; Schiaffino & Sonin 1996*a*, *b*). Gao & Sonin found that they could produce uniform beads when the contact angle was small, but that beads with higher effective contact angles developed marked undulations before solidifying.

Our present experiments were undertaken to establish quantitatively the conditions under which uniform beads will occur in sweep deposition of molten materials, and to examine how the beads, stable or unstable, actually form. An adapted molten-wax ink-jet printer head of the drop-on-demand type was used to generate 50 μm diameter droplets of a molten microcrystalline wax (Reed 6882) at frequencies f in the range 0.5–15 kHz. The droplets arrived at the target with a speed of about 2.5 m s^{-1}. The target was Plexiglas, which has thermal properties roughly similar to the wax. Table 1 gives the physical properties of the wax and the target material (see also Gao & Sonin's comments about the melting point of the microcrystalline wax). In the experiments cited here, the sweep speed U ranged from 0.5 to 50 mm s^{-1}. The droplet temperature T_0 at impact was 14 °C above the melt's fusion point in all tests, and the target temperature T_t was 20–60 °C below the fusion point. The Bond number $\rho g R^2/\sigma$ based on the bead's transverse radius of curvature was in all cases small, usually of order 10^{-3}–10^{-2}, and gravitational effects were thus negligible. The deposited bead was observed via a microscope fitted with a CCD camera both during deposition, in which case the camera would be moved either with the droplet generator or the target, and after the experiment when the bead had solidified. The bead's contact lines could be observed and measured from below through the transparent target.

Figures 3 and 4 show some solid beads obtained by sweep deposition at relatively high target temperatures where the beads had low or moderate contact angles. Smooth, uniform beads were obtained, shaped like segments of a cylinder with essentially

https://doi.org/10.1017/S0022112097005831 Published online by Cambridge University Press

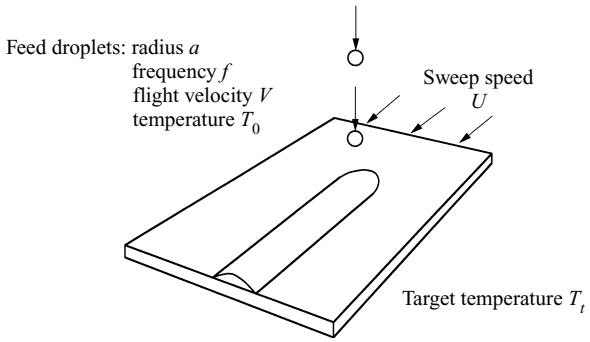


FIGURE 2. Schematic illustration of sweep deposition and its operational parameters.

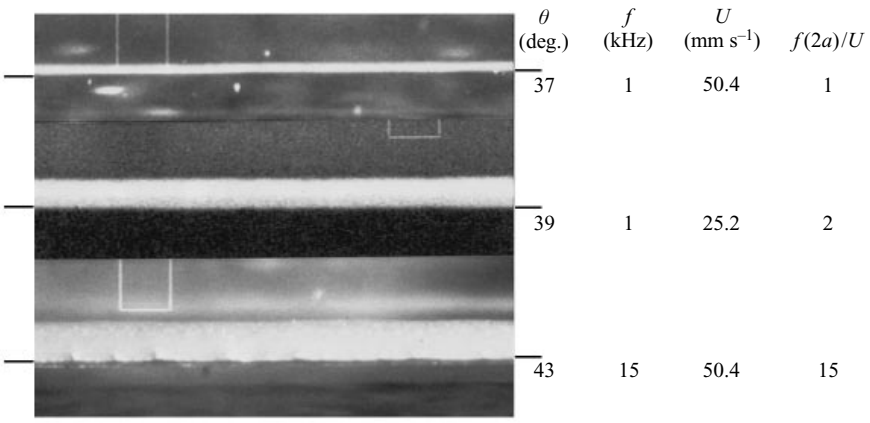


FIGURE 3. Stable beads observed from the side. Microcrystalline wax on Plexiglas. $T_0 = 105$ °C, $T_t = 70$ °C. The rectangle's width is 200 μm. In this and the following pictures, the black lines on the sides indicate the elevation of the target.

Material	Thermal conductivity k (W m^{-1} K^{-1})	Density ρ (kg m^{-3})	Specific heat c (J kg^{-1} K^{-1})
Microcrystalline wax	0.12	9.3×10^2	2.1×10^3
Plexiglas target	0.15	1.2×10^3	1.3×10^3

TABLE 1. Properties of the melt and target materials. The wax has a melting point of 90 °C, latent heat of fusion $L = 2 \times 10^5$ J kg^{-1}, viscosity $\mu = 1.8 \times 10^{-2}$ kg m^{-1} s^{-1} at 90 °C decreasing to 1.4×10^{-2} kg m^{-1} s^{-1} at 105 °C (Schiaffino 1996), and surface tension $\sigma = 0.025$ N m^{-1} (Gao & Sonin 1994).

constant base width (see figure 4). For this shape the base width is related to the apparent contact angle via (Gao & Sonin 1994, equation (35))

$$\frac{b}{2a} = \left(\frac{2\pi \sin^2\theta}{3(\theta - \sin\theta\cos\theta)} \frac{f(2a)}{U} \right)^{1/2} \tag{1}$$

where a and f are the microdrop radius and deposition frequency, and U is the sweep speed. The contact angles indicated in the figures are calculated from (1) based on post-deposition (i.e. final solid state) measurements of the base width b, the other

https://doi.org/10.1017/S0022112097005831 Published online by Cambridge University Press

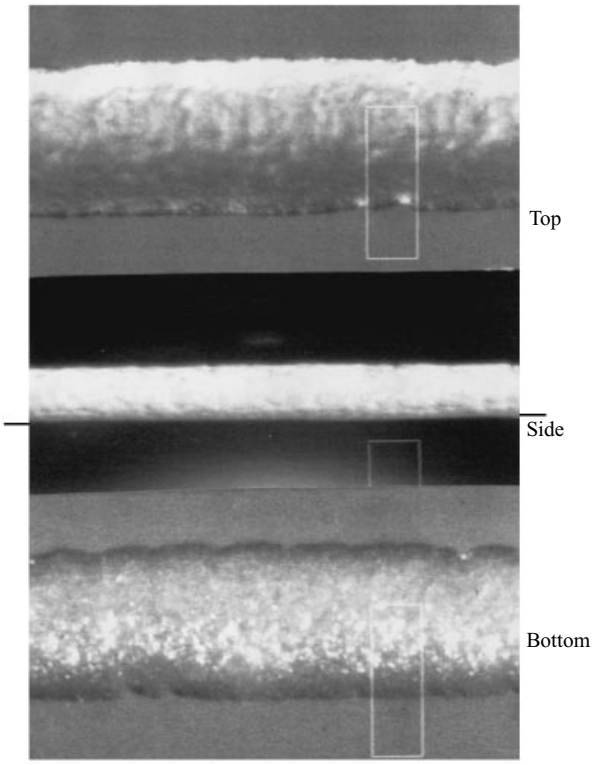
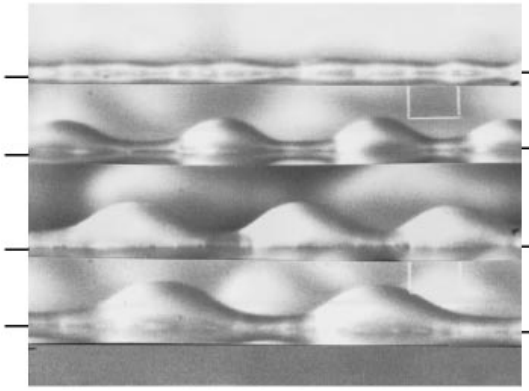


FIGURE 4. A stable bead observed from different directions. Microcrystalline wax on Plexiglas. $T_0 = 105$ °C, $T_t = 70$ °C, $f = 10$ kHz, $U = 50.4$ mm s^{-1}, $f(2a)/U = 9.9$, $\theta = 47°$. The rectangle's width is 100 μm.



θ (deg.)	f (kHz)	U (mm s^{-1})	$f(2a)/U$
115	2	50.4	2.0
118	5	50.4	5.0
135	10	50.4	9.8
138	10	40.6	12.3

FIGURE 5. Unstable beads observed from the side. Microcrystalline wax on Plexiglas. $T_0 = 105$ °C, $T_t = 35$ °C. The rectangle's width is 200 μm.

parameters being known. The contact angles are below $\frac{1}{2}\pi$ for all the stable beads of figures 3 and 4, consistent with Davis's (1980) theory for beads with arrested contact lines.

Figures 5 and 6 show beads formed at lower target temperatures, where the post-solidification contact angle exceeded $\frac{1}{2}\pi$. These beads also have approximately constant base width (figure 6, bottom view), but their profiles show marked undulations similar to those observed by Gao & Sonin. For these beads the apparent contact angle θ

https://doi.org/10.1017/S0022112097005831 Published online by Cambridge University Press

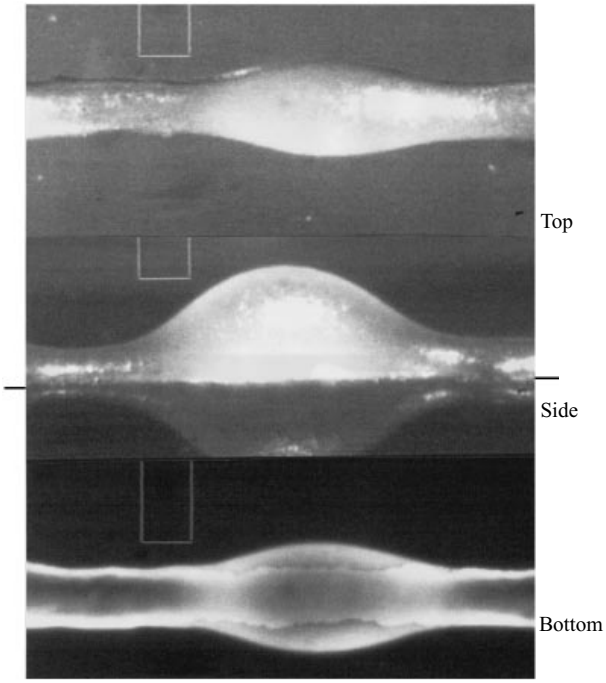


FIGURE 6. A bulge in an unstable bead, observed from different directions. Microcrystalline wax on Plexiglas. $T_0 = 105$ °C, $T_t = 35$ °C, $f = 10$ kHz, $U = 40.6$ mm s^{-1}, $f(2a)/U = 12.3$, $\theta = 138°$. The rectangle's width is 100 μm.

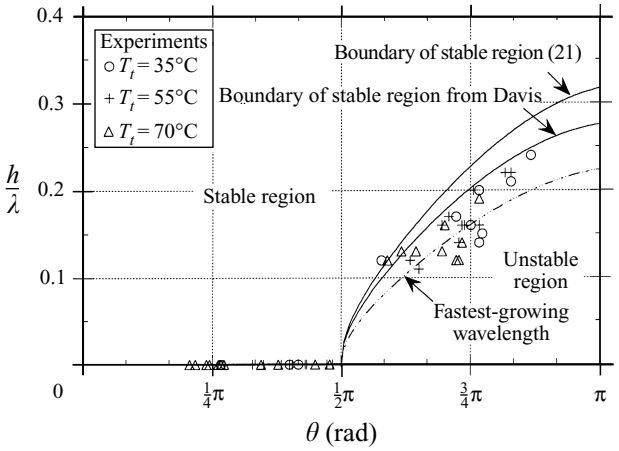


FIGURE 7. Stable and unstable regions for beads with parallel, arrested contact lines; experiments for molten wax.

indicated in the figures is the *nominal* value, computed by using the measured base width in (1). The nominal θ is the contact angle of a *uniform* bead with the same base width and same average mass per unit length as the actual bead. All the beads in figures 5 and 6 have $\theta > \frac{1}{2}\pi$, and are thus in the regime where theory predicts instability.

In figure 7 we plot all our experimental data for h/λ vs. θ, where h is the bead height and λ is the *average* undulation wavelength, taken over at least 15 wavelengths, in the case of unstable beads. Beads judged to be uniform are represented as having $h/\lambda = 0$.

https://doi.org/10.1017/S0022112097005831 Published online by Cambridge University Press

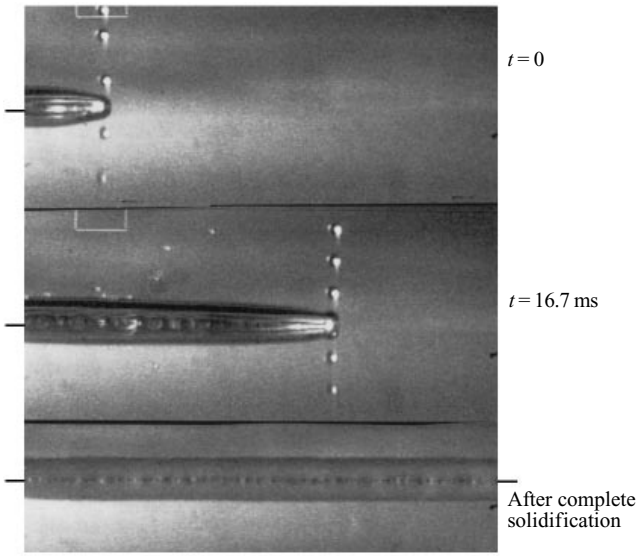


FIGURE 8. Video sequence of a stable bead formed by sweep deposition (side views). The pictures are obtained with strobe lighting. The frame interval is 1/60 s. The camera is fixed in the reference frame of the target and the droplet generator is moving from left to right. Microcrystalline wax on Plexiglas. $\theta = 43°$, $T_0 = 105$ °C, $T_t = 70$ °C, $f = 15$ kHz, $U = 50.4$ mm s^{-1}, $f(2a)/U = 15$. The rectangle's width is 200 μm.

For non-uniform (unstable) beads h is calculated from the measured fixed base width b and the nominal θ using

$$h = b(1-\cos\theta)/2\sin\theta. \tag{2}$$

Consistent with Davis's theory for beads with fixed, parallel contact lines, all beads with $\theta < \frac{1}{2}\pi$ are stable, and all those with $\theta > \frac{1}{2}\pi$ are unstable. We shall see that the observed instabilities have wavelengths which are approximately equal to the fastest-growing wavelength, as given by the theory presented in the next section.

Both Davis's theory and our theory of §4 below are formulated for instabilities developing in an 'infinite' bead which originally has a uniform cross-section (figure 1). The experiments show, however, that the instabilities actually develop right at the bead head as the liquid is laid down. Figure 8 shows the bead formation process for a *stable* bead. The successive video frames (strobe-illuminated) are side views, taken as the bead's head passes a camera fixed in the target's reference frame. The Plexiglass target acts as a mirror, and the pictures show the bead and its reflection below; the target plane is in the middle of the two. The strobe lighting catches the stream of incoming microdrops. A microdrop arrives at the head, breaks the melt interface at the first point of contact, and surface tension then propels its liquid into the bead, slingshot-fashion, with a velocity of order $(\sigma/\rho a)^{1/2}$ which is approximately 1 m s^{-1} in our case, much faster than the target's sweep speed U. The drop is swallowed into the bead in a time of order $(\rho a^3/\sigma)^{1/2}$, 25 μs in this case, about one-third of the time between successive drop arrivals. In this case deposition is steady in a reference frame moving with the bead's head. The bead reaches a stable height h at a distance of the order of a few h downstream in this case, indicating that the melt velocity has slowed to the target velocity at that point. The viscous development length based on target speed U, Uh^2/ν, is only about $0.3h$.

Bead formation under *unstable* conditions is very different (figure 9). Undulations form immediately downstream of the head and, in the reference frame of the bead

https://doi.org/10.1017/S0022112097005831 Published online by Cambridge University Press

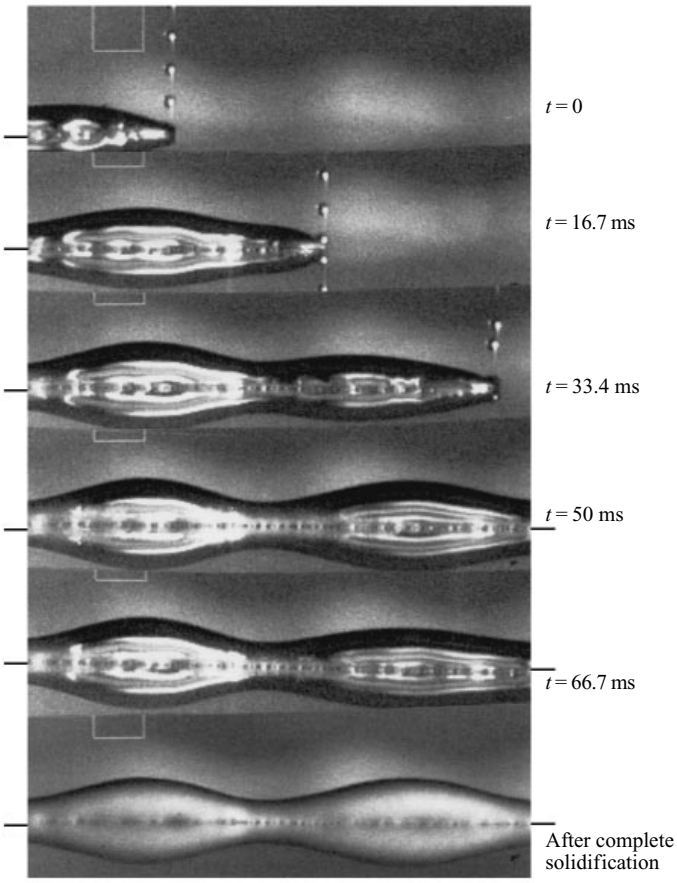


FIGURE 9. Video sequence of an unstable bead formed by sweep deposition, obtained as in figure 8. Microcrystalline was on Plexiglas. $T_0 = 105$ C, $T_i = 35$ °C, $f = 15$ kHz, $U = 37.8$ mm s^{-1}, $f(2a)/U = 20$. The square's side is 200 μm.

head, the shape oscillates both temporally and spatially with large amplitude. Liquid is deposited on the target as the head moves over it. Every time the head advances by a distance about equal to the fastest-growing wavelength from the head (see §4), a bulge starts to grow but is pinched off abruptly as its wavelength stretches beyond the value associated with the maximum growth rate region. The pinched-off bulge then remains on the target while a new bulge starts forming at the head.

The primary effect of solidification is to provide the conditions that lead to the arrest of the contact lines at a constant separation. Sweep deposition with water droplets, for example, will not form such a bead, largely because water tends to maintain an approximately constant contact angle with the target, no matter which way the contact line moves, and is therefore always unstable in a cylindrical configuration. When a molten material is deposited, the droplets coalesce on the target and the melt wets the target and spreads laterally as it is carried downstream on the target. The lateral spreading soon stops because the contact lines are arrested by freezing once they slow down sufficiently (Schiaffino & Sonin 1996*a*, *b*). The bead's apparent contact angle at this point depends strongly on target subcooling, the angle increasing with increasing subcooling. We are left with a bead which has arrested, parallel contact lines, but is otherwise still liquid everywhere except very near its bottom. If conditions are unstable,

https://doi.org/10.1017/S0022112097005831 Published online by Cambridge University Press

the liquid will subsequently redistribute itself axially, and the apparent (macroscopic) contact angle will seem to increase under a bulge and decreases under a trough, but the contact lines tend to stay arrested once they have stopped moving.

The role of bulk solidification in the deposition process can be assessed by estimating the average thickness δ of the solidification layer which penetrates into the melt from below (the heat loss into the air is small). δ can be estimated by applying Carslaw & Jaeger's (1959) solution for one-dimensional transient solidification at the interface between a semi-infinite melt and a semi-infinite subcooled solid. This yields

$$\delta(r, t) = \xi(\alpha t)^{1/2}, \tag{3}$$

where t is the time after contact, α is the material's thermal diffusivity, and the coefficient ξ depends on the materials' properties and initial temperatures and is given by Carslaw & Jaeger. For constant properties between the melt and solid (a fair approximation in our case: see Table 1) and for $\xi/2 \ll 1$ one obtains the simple result

$$\xi = \frac{2}{\pi^{1/2}} \frac{c(T_f - T_t)}{L} \left(1 - \frac{T_0 - T_f}{T_f - T_t}\right), \tag{4}$$

where c is the melt's (and target's) specific heat, L is the melt's latent heat of fusion, and $(T_0 - T_f)/(T_f - T_t)$ is the ratio of the melt's superheat to the target's subcooling. If the target has approximately the same thermal properties as the molten material, as we have assumed, but does not melt, as in our experiments with Plexiglass, (3) applied only if $(T_0 - T_f)/(T_f - T_t) < 1$, which corresponds to conditions where the host phase solidifies. To apply this solution to our bead we set $t = x/U$, where x is the distance downstream from the head, and obtain

$$\delta_s = \xi(\alpha x/U)^{1/2}. \tag{5}$$

Carslaw & Jaeger's model with two semi-infinite materials applies to our case as long as the thermal diffusion layer thickness $\delta_T = (\alpha x/U)^{1/2}$ is small compared with both the bead's height h and base width b. This is the case for the bead in figure 9, for which (4) and (5) give $\delta_s \approx 20$ μm at the downstream end of the first wave, or about one quarter of the local bead height.

Solidification does not, therefore, control the initial growth of the instability in figure 9. It may, however, determine its final amplitude. The growth of the undulations will be arrested by one of two mechanisms, whichever occurs first: either solidification will penetrate the troughs, or the system will reach a new stable deformation with finite peak-to-trough height ratio. The latter occurs as follows. When an unstable deformation ($\theta > \frac{1}{2}\pi$) begins, the transverse interfacial curvature will be higher at points where h is lower, and liquid will move from those points and depress the local h further. After the low points are depressed so much that the local contact angle reaches $\frac{1}{2}\pi$, however, their transverse curvature will begin to decrease upon further height reduction and will continue to do so until the pressure difference which amplifies the disturbance reaches zero. This represents a new stable configuration with finite amplitude. An idealized inviscid theory would end up oscillating about this configuration, but a real viscous fluid will reach it.

3. Experiments with water

Liquids which have freely moving contact lines do not form beads when a droplet stream is swept over a surface, even if successive droplets overlap on impact. Figure 10 shows a side view of what happens when 50 μm diameter water droplets are deposited

https://doi.org/10.1017/S0022112097005831 Published online by Cambridge University Press

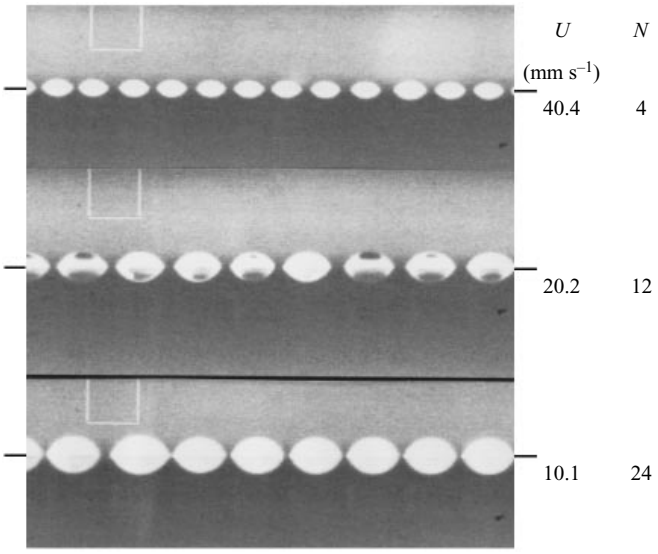


FIGURE 10. Sessile macrodrops of water on Plexiglas obtained by sweep deposition. N is the number of coalesced microdrops which form each of the separate macrodrops. $f = 1$ kHz. The rectangle's breadth is 200 μm.

on a Plexiglas surface at 1 kHz at various sweep speeds, all of which are low enough for successive droplets to overlap on impact (see Gao & Sonin 1994, equations (30) and (31)). Instead of beads, sessile drops are formed, their size dependent on sweep speed and deposition frequency. (Note again that the picture shows not only the sessile drops but their mirror images below, reflected in the transparent Plexiglas surface.) Water on Plexiglas tends to maintain a constant contact angle, and, as a result, when a newly arriving microdrop touches the previous one on the surface, the two will rapidly coalesce and form a single sessile droplet. The inertially limited time scale for this is $(\rho a^3/\sigma)^{1/2}$, about 20 μs in this case, much shorter than the 1 ms time between the arrival of successive microdrops. If the third droplet misses the coalesced pair, it will become the seed for a next pair, and a row of sessile drops consisting of two microdrops will form. At lower advance speeds, the sessile macrodrops will consist of three, four or more microdrops. In figure 10, for example, the macrodrops contain approximately 4, 12, and 24 microdrops at $U = 4.0$, 2.0 and 1.0 cm s^{-1}, respectively.

The coalescence of two successive microdrops into a larger drop is caught in the strobe-lighted sequence of figure 11. A microdrop approaches the target (note its mirror image again!) close to the sessile drop which has preceded it. The new microdrop lands on the target ahead of its predecessor, spreads to take on a sessile form, touches the previously formed sessile drop, and the two rapidly coalesce. The whole sequence lasts about 20 μs. The next microdrop will miss this pair and become the seed for a new pair.

Clearly, since beads with constant contact angle are invariably unstable, contact line mobility can completely defeat attempts to form beads from liquids. This is true whether the liquid is deposited as droplets or as a continuous stream (e.g. from the tip of a syringe drawn across a surface). Beads will form if there is a sufficient degree of contact line hysteresis; contact line arrest is a limiting case of hysteresis. Beads will also form if the capillarity-driven spreading of the liquid is sufficiently slow (e.g. the liquid is sufficiently viscous) and if the spreading can be halted by some means (e.g. by phase change or chemical reaction) before the bead develops instabilities and breaks up.

https://doi.org/10.1017/S0022112097005831 Published online by Cambridge University Press

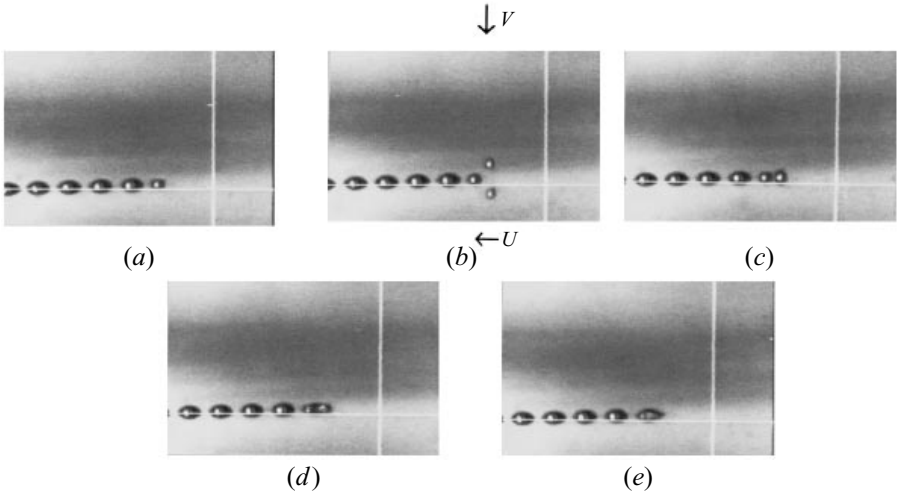


FIGURE 11. Video sequence obtained with strobe illumination for sweep deposition of water droplets on a Plexiglas target, showing the coalescence of a newly arriving microdrop with the previous one to form a doublet. The camera is fixed in the reference frame of the droplet generator and the target moves from right to left. $f = 60$ Hz, $U = 4$ mm s^{-1}, $f(2a)/U = 0.75$. (*a*) $t = -16.7$ ms, (*b*) $t = 0$, (*e*) $t = 20$ μs.

4. Theory for the dominant instability wavelength

Davis's (1980) methodology does not lend itself straightforwardly to a determination of the instability's dispersion relation and the wavelength associated with most rapid growth, which determines what one observes. We shall establish these with a simpler model. The liquid flow is taken as inviscid, incompressible, and quasi-one-dimensional, and gravitational effects are neglected, the assumption being that the Bond number $Bo = \rho g R^2/\sigma$ based on the bead's transverse radius of curvature is sufficiently small. The equations of motion and mass conservation are

$$\rho\left(\frac{\partial u}{\partial t} + u\frac{\partial u}{\partial x}\right) = -\frac{\partial p}{\partial x}, \tag{6}$$

$$\frac{\partial A}{\partial t} + u\frac{\partial A}{\partial x} = -A\frac{\partial u}{\partial x}, \tag{7}$$

where A is the bead's cross-sectional area, u is the flow velocity in the x-direction, t is time, ρ is the liquid density, and p is the pressure inside the bead. Gravitational effects being negligible, the bead's cross-section in a plane transverse to the x-axis is modelled as a segment of a circle with radius $R(x)$ (see figure 1*a*), and the gauge pressure at x is written as

$$p = \sigma(1/R + 1/R') \tag{8}$$

where σ is the liquid's surface tension and $1/R'$ is the *average* value of the longitudinal curvature of the bead's surface at station x. These approximations are consistent with quasi-one-dimensional flow, where $p \approx p(x, t)$, and simplify the analysis greatly while retaining a realistic representation of the main features of the physics. The area A in (7) can be expressed straightforwardly in terms of the bead's local contact angle θ and local height h above the centreline as

$$A = h^2(\theta - \sin\theta\cos\theta)/(1 - \cos\theta)^2. \tag{9}$$

https://doi.org/10.1017/S0022112097005831 Published online by Cambridge University Press

The radius R can be expressed either in terms of θ and h as

$$R = h/(1-\cos\theta) \tag{10}$$

or in terms of θ and the bead's base width b as

$$R = b/(2\sin\theta). \tag{11}$$

We simplify our analysis further by writing the average longitudinal curvature as

$$1/R' \approx -\beta\,\partial^2 h/\partial x^2, \tag{12}$$

where $-\partial^2 h/\partial x^2$ is the curvature of the surface over the centreline, the assumption being one of small slope, and β is a coefficient which corrects for the difference between the longitudinal curvature over the centreline and the average longitudinal curvature. The calculation of β is described by Schiaffino (1996). We use a constant β which is the average value over the whole bead surface for a small-amplitude perturbation. This average value is independent of the perturbation amplitude, but depends on the bead's initial unperturbed shape (i.e. contact angle) and on how the bead's contact line responds to the perturbation. In what follows, we apply our analysis to two limiting cases of contact line behaviour: the case where the contact lines are arrested at a constant separation b while the contact angle is free to change, and the case where the bead maintains a fixed contact angle θ while its two contact lines are free to move (figure 1). Since b is fixed in the first case, and θ is fixed in the second, $A = A(h)$ and $R = R(h)$ in both, and we obtain from (6)–(8) and (12), for both cases,

$$\frac{\partial u}{\partial t} = \frac{\sigma}{\rho}\left(\frac{1}{R^2}\frac{\mathrm{d}R}{\mathrm{d}h}\frac{\partial h}{\partial x} + \beta\frac{\partial^3 h}{\partial x^3}\right), \tag{13}$$

$$\frac{\mathrm{d}A}{\mathrm{d}h}\frac{\partial h}{\partial t} = -A\frac{\partial u}{\partial x}, \tag{14}$$

where we have neglected the convective terms, consistent with the assumption of small perturbations.

We now write the bead's height as

$$h = h_0 + \epsilon\,\mathrm{e}^{\omega t + \mathrm{i}kx} \tag{15}$$

where h_0 is the bead's unperturbed height, ϵ is the amplitude and k the wavenumber of the height perturbation imposed at $t = 0$, and ω is the inverse timescale of the disturbance growth. Using (15) in (13) and (14) we obtain the velocity perturbation as

$$u = \frac{\mathrm{i}\epsilon\sigma k}{\rho\omega}\left(\frac{1}{R^2}\frac{\mathrm{d}R}{\mathrm{d}h} - \beta k^2\right)\mathrm{e}^{\omega t + \mathrm{i}kx} \tag{16}$$

and the dispersion relation for the shape perturbation growth as

$$\omega^2 = \frac{\sigma k^2 A}{\rho\,\mathrm{d}A/\mathrm{d}h}\left(\frac{1}{R^2}\frac{\mathrm{d}R}{\mathrm{d}h} - \beta k^2\right). \tag{17}$$

Equation (17) shows that the system is stable if

$$k^2 > \frac{1}{\beta R^2}\frac{\mathrm{d}R}{\mathrm{d}h} \tag{18}$$

and that the maximum unstable growth rate occurs at a wavenumber k_* given by

$$k_*^2 = \frac{1}{2\beta R^2}\frac{\mathrm{d}R}{\mathrm{d}h}. \tag{19}$$

https://doi.org/10.1017/S0022112097005831 Published online by Cambridge University Press

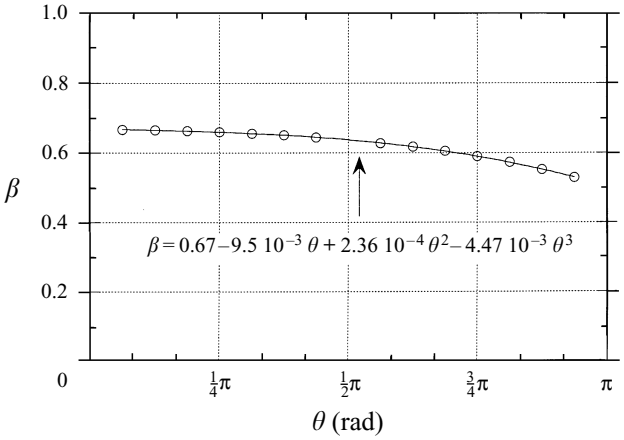


FIGURE 12. The coefficient β for beads with parallel, arrested contact lines.

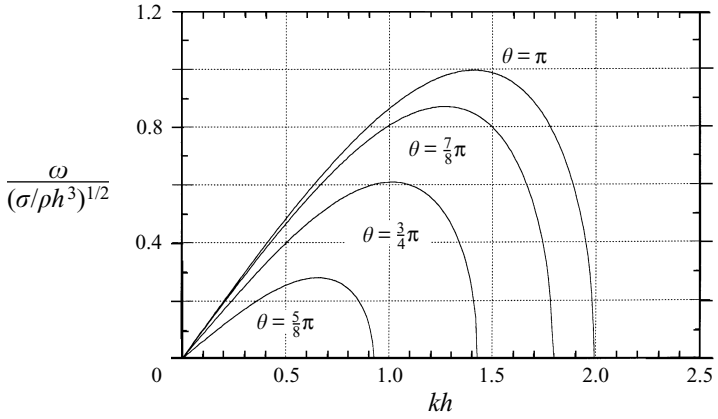


FIGURE 13. Dispersion relation for beads with parallel, arrested contact lines.

It is worth noting that our quasi-one-dimensional flow approximation gives a quite accurate answer to Rayleigh's well-known problem of the infinite liquid cylinder, which our equations describe if we set $h \equiv R$, $\beta = 1$, and $A = \pi R^2$. With these substitutions (14) predicts a fastest-growing unstable wavelength of $\lambda_* = 2\pi k_* = 2\sqrt{2}\,\pi R = 8.88R$, which differs from Chandrasekhar's (1961) value of $9.02R$ by less than 2%.

4.1. *Parallel, arrested contact lines*

For a bead with its two contact lines arrested at a fixed separation b, $R(h)$ is obtained by eliminating θ between (10) and (11) and $A(h)$ by eliminating θ between (9) and (2). From these we obtain $\mathrm{d}R/\mathrm{d}h$ and $\mathrm{d}A/\mathrm{d}h$ and then from (17) the dispersion relation

$$\frac{2\rho h^3\omega^2}{\sigma} = \frac{(kh)^2[\theta - \sin\theta\cos\theta]\,[\cos\theta\,(\cos\theta - 1) - \beta(kh)^2]}{\sin\theta - \theta\cos\theta}. \tag{20}$$

The stable region is defined by

$$(kh)^2 > \cos\theta\,(\cos\theta - 1)/\beta \tag{21}$$

which shows that a bead with arrested contact lines is always stable when $\theta < \frac{1}{2}\pi$, while when $\frac{1}{2}\pi < \theta < \pi$ there are always unstable wavelengths. The computed value of β for this case is shown in figure 12, and figure 13 shows the corresponding dispersion

https://doi.org/10.1017/S0022112097005831 Published online by Cambridge University Press

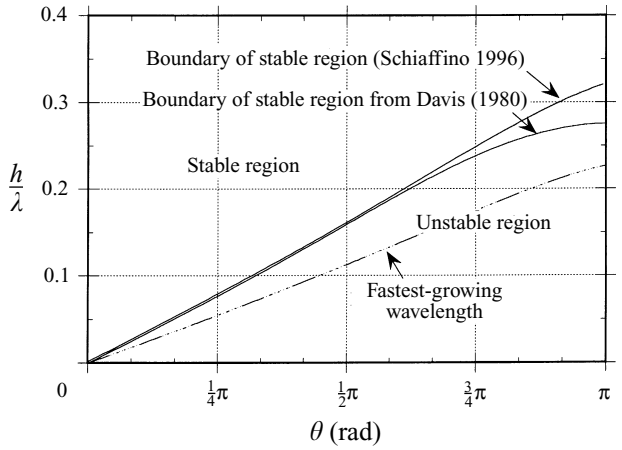


FIGURE 14. Stable and unstable regions for beads with constant contact angle θ.

relationship for unstable conditions. As θ increases, the range of unstable wavenumbers increases.

Figure 7 displays, on a map of wavelength $\lambda = 2\pi/k$ vs. θ, the region of unstable growth and the most rapidly growing wavenumber k_*. The latter is given by

$$(k_* h)^2 = \frac{\cos\theta\,(\cos\theta - 1)}{2\beta}. \tag{22}$$

The inverse timescale ω_* of the fastest-growing unstable wavenumber is obtained from (20) and (22) as

$$\frac{\rho h^3 \omega_*^2}{\sigma} = \frac{\cos^2\theta\,(\cos\theta - 1)^2(\theta - \sin\theta\cos\theta)}{8\beta\,(\sin\theta - \theta\cos\theta)}. \tag{23}$$

A stable region exists in this case because, with arrested contact lines and $\theta < \frac{1}{2}\pi$, the transverse curvature is higher in locations where the bead elevation h is higher. This raises the internal pressure and moves the liquid away from those regions, thus reducing the perturbation. The opposite is true if $\theta > \frac{1}{2}\pi$.

We note in figure 7 that Davis's (1980) stability boundary falls approximately 10 % lower than ours over the range of unstable conditions ($\frac{1}{2}\pi < \theta < \pi$). The discrepancy presumably arises because of our simplifying assumptions (quasi-one-dimensional flow and small interfacial slope) which lose accuracy in the region where h/λ is not small.

4.2. *Bead with constant contact angle*

The case where θ retains a fixed value regardless of the contact line dynamics is, as we have seen, of less practical importance. It is always unstable, just like Rayleigh's liquid cylinder. For this reason, the liquid will in typical cases – or, at least, those where our inviscid analysis is relevant – break up into sessile droplets as it is laid down, and never take on the shape of a bead, the assumed initial condition in a stability analysis.

Our solution for the bead with constant contact angle is given by Schiaffino (1996). Figure 14 shows the stable and unstable regions on a map of h/λ vs. θ, where $\lambda = 2\pi/k$ is the perturbation wavelength. The fastest-growing wavenumber k_* is given by

$$(k_* h)^2 = (1 - \cos\theta)/2\beta. \tag{24}$$

Again, our neutral stability curve falls somewhat below that of Davis (1980) at θ

https://doi.org/10.1017/S0022112097005831 Published online by Cambridge University Press

greater than $\frac{3}{4}\pi$, say. Sekimoto *et al.* (1987) developed a static morphological analysis of partial wetting and applied it to a bead with constant but small ($\theta \ll 1$) contact angle. For the varicose instability mode which corresponds to our present analysis, their analysis (see their equation (4.23)) yields for small Bond numbers essentially the same result for the neutral stability curve as both Davis's and ours.

5. Comparison of experiment and instability theory

The experimental data for molten wax are in satisfactory accord with the inviscid theory for beads with parallel, arrested contact lines, which is in fact what these beads had. All beads with $\theta < \frac{1}{2}\pi$ are stable, all those with $\theta > \frac{1}{2}\pi$ are unstable, and the observed instabilities have wavelengths consistent (within the data scatter) with the fastest-growing wavelength of the theory, (22).

This agreement leaves us one question: was the flow indeed approximately inviscid in these experiments? Viscous effects will not affect the result that a bead with parallel, arrested contact lines is stable if $\theta < \frac{1}{2}\pi$ and unstable at some wavelengths if $\theta > \frac{1}{2}\pi$. Viscosity will, however, affect the fastest-growing wavelength. The timescale for the fastest-growing instability to develop is ω_*^{-1}, where ω_* is given by (23) for inviscid flow. The criterion for inviscid instability development is thus $h^2\omega_*/\nu \gg 1$ where ν is the liquid's kinematic viscosity. In the unstable region the magnitude of $h^2\omega_*/\nu$ ranged from about unity closest to $\theta = \frac{1}{2}\pi$ to about 15 at the highest θ. Inviscid flow is thus a fair assumption at least for the data at the higher θ. The criterion for inviscid flow becomes increasingly difficult to satisfy as θ approaches $\frac{1}{2}\pi$ from above because $\omega_* \to 0$ as $\theta \to \frac{1}{2}\pi$. In practice, however, the instability has already developed a significant amplitude in the bead formation stage rather than after a uniform bead has been laid down (as is implied in the instability analysis) and this will tend to speed up its formation.

6. Conclusions

Theory predicts that a liquid bead deposited on a flat solid is unstable if its contact lines move at a fixed contact angle; if the contact lines are arrested, however, the bead is stable if the initial contact angle is less than $\frac{1}{2}\pi$ and unstable if greater than $\frac{1}{2}\pi$. Our experiments show that a molten bead can be deposited by sweeping a stream of molten microdrops over a cold, solid substrate. Such beads tend to form with parallel, arrested contact lines while the bulk of the bead remains in the liquid state long enough after deposition to develop instabilities under conditions where these tend to occur. An inviscid theory adequately predicts both the conditions of instability and its wavelength for wax beads. The beads' apparent contact angle was found to depend strongly on the target's subcooling (the difference between the melt's fusion temperature and the far-field target temperature), the angle increasing with increasing subcooling.

No beads could be formed with similarly deposited droplets of water, which tend to maintain a fixed contact angle with Plexiglas. Instead, a series of separate macrodrops would form, each composed of a certain number of microdrops. Contact line arrest, or at least hysteresis, is a prerequisite for bead formation from liquid droplets.

This research was supported by the National Science Foundation under grants CTS-9413026 and 9523764.

https://doi.org/10.1017/S0022112097005831 Published online by Cambridge University Press

REFERENCES

Carslaw, H. S. & Jaeger, J. C. 1959 *Conduction of Heat in Solids*, 2nd Edn. Clarendon Press.

Chandrasekhar, S. 1961 *Hydrodynamic and Hydromagnetic Stability*. Clarendon Press. (Also Dover, 1981.)

Davis, S. H. 1980 Moving contact lines and rivulet instabilities. Part 1. The static rivulet. *J. Fluid Mech.* **98**, 225–242.

Gao, F. & Sonin, A. A. 1994 Precise deposition of molten microdrops: the physics of digital microfabrication. *Proc. R. Soc. Lond.* A **444**, 533–554.

Rayleigh, Lord 1878 On the stability of jets. *Proc. Lond. Math. Soc.* **10**, 4–13.

Schiaffino, S. 1996 The fundamentals of molten microdrop deposition and solidification. PhD thesis, Department of Mechanical Engineering, MIT.

Schiaffino, S. & Sonin, A. A. 1997*a* Motion and arrest of a molten contact line on a cold surface: an experimental study. *Phys. Fluids* (in press).

Schiaffino, S. & Sonin, A. A. 1997*b* On the theory for the arrest of an advancing molten contact line on a cold solid of the same material. *Phys. Fluids* (in press).

Sekimoto, K., Oguma, R. & Kawasaki, K. 1987 Morphological stability analysis of partial wetting. *Ann. Phys.* **176**, 359–392.

https://doi.org/10.1017/S0022112097005831 Published online by Cambridge University Press